Chapter 6

Synthesis and Characterization of Reduced Graphene Oxide/Polyaniline/Au Nanoparticles Hybrid Material for Energy Applications

Carmina Menchaca-Campos, Elsa Pereyra-Laguna, César García-Pérez, Miriam Flores-Domínguez, Miguel A. García-Sánchez and Jorge Uruchurtu-Chavarín

Additional information is available at the end of the chapter

http://dx.doi.org/10.5772/intechopen.77385

Abstract

In this work, synthesis and characterization of reduced graphene oxide/polyaniline/Au nanoparticles (GO/PANI/NpAu) as a hybrid capacitor are presented. Graphite oxide (GO) was synthesized by a modified Hummer's method. Polyaniline was synthesized by chemical polymerization, and Au nanoparticles (NpAu) were added afterward. Fabrication of the electrodes consisted on the hybrid materials being deposited on carbon cloth electrodes. The chemical and structural properties of the electrode were characterized by high-resolution scanning electron microscopy (HRSEM), Fourier transform infrared spectroscopy (FTIR), X-ray diffraction (X-R), and Raman spectroscopy; the results confirm the graphene reduction, the covalent functionalization, and formation of nanocomposites and also show the polyaniline grafted graphene. The performance and evaluation of the electrodes based on grapheme oxide (GO), polyaniline (PANI), GO-PANI, and GO/PANI/NpAu nanocomposites over carbon cloth, stainless steel, and copper have been obtained in 1 M H_2SO_4 solution, using electrochemical techniques namely: cyclic voltammetry (CV) and electrochemical impedance spectroscopy (EIS). They showed that GO/PANI/NpAu gave higher specific capacitance (SC) and energy values than PANI, and GO/PANI, in the order of 160 F/g. The present study introduces new hybrid material for energy applications, from the evaluation of their electrical contributions.

Keywords: graphene oxide, polyaniline, gold nanoparticles, electrochemical, redox

1. Introduction

With climate change and environmental concern, new energy sources have been created and various advanced energy storage systems. They simultaneously possess high energy and high power density as well as excellent recyclability, low cost, and friendly to the environment [1].

There are energy storage devices such as lithium-ion batteries often possessing high energy (200 Wh/Kg) but relatively low power density (1 KW/Kg), while traditional electrostatic capacitor has high power (40 KW/Kg) but low energy density (0.03 Wh/Kg) [2]. However, the electrochemical capacitor is a new type of high power and high energy density storage and deliverance device, therefore promising for feeding a variety of equipment operating with energy [3].

The capacitors can be divided into two classes based on charge-storage mechanism: (a) electrical double layer capacitors (EDLCs), where in electrode/electrolyte system, direction arrangement of the electron, or ion at the electrode/electrolyte interface forms electrical double layer [4] and (b) pseudo-capacitors, where the pseudo-capacitance arises from Faradaic reactions taking place at the electrode/electrolyte interface [5].

From the basic characteristics that determine the development of high-performance electrochemical capacitor (EC) electrodes, the most important are design, manufacture electrodes with suitable materials, architecture, and structure [2].

The typical electrode materials for EDLC are carbon materials (carbon nanotubes, graphene, activated carbon, etc.) due to their high-specific surface area and excellent conductivity [6], and the conductive polymers (polypyrrole, polyaniline, and polythiophene) are often used for pseudo-capacitors due to their high conductivity and large storage capacity [7]. However, the specific capacitance of carbon materials is commonly far less than that of conductive polymers, and the storage capacity of conductive polymers gradually decreases with the increase in the number of cycle (charge-discharge) [4].

In order to alleviate the inherent drawback of single materials, researchers have combined carbon materials and conductive polymers to obtain hybrid or composite materials with both high-specific capacitance and good cycle life called hybrid supercapacitors [8].

There are two methods for the preparation of hybrid capacitors: chemical methods in which an oxidizing agent is used and in-situ polymerization occurs, e.g., in situ chemical polymerization of graphene with polyaniline [9], forming the hybrid composite graphene/polyaniline (**Figure 1**). Another method is the electrochemical synthesis of conductive polymeric nanocomposites in which nanomaterials are dispersed in a monomer solution and formed by electropolymerization [10].

Being Au an excellent conductive material, it can be used to improve further the electrical properties of the GO/PANI hybrid material, incorporating it into the polymer matrix, as gold nanoparticles (NpAu), expecting the nanoscale dimension to potentiate the overall hybrid material properties.

With all the above ideas in mind, the next section shows some results about the synthesis of graphene oxide/polyaniline/Au nanoparticles hybrid material suitable to be used for energy applications.

http://dx.doi.org/10.5772/intechopen.77385

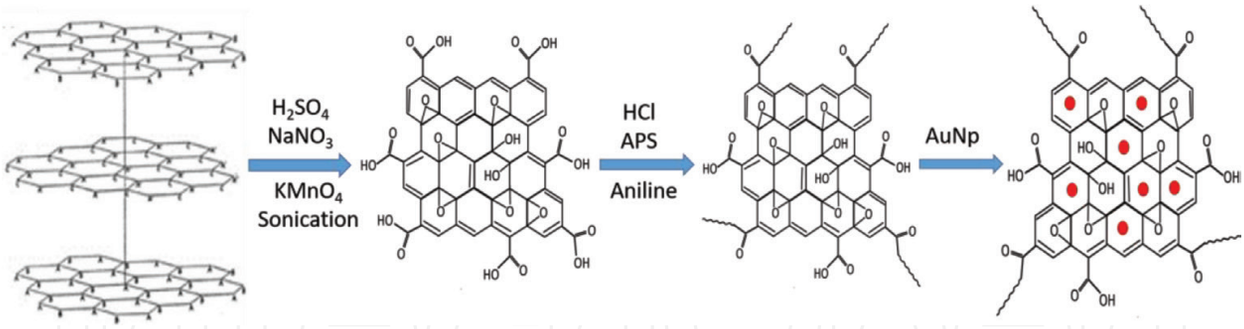

Figure 1. In situ polymerization of graphene oxide with polyaniline, forming the hybrid composite graphene oxide/polyaniline, and the incorporation of AuNp on the matrix GO/PANI.

2. Methodology development

The systems discussed were synthesized by the methodology, as shown in **Figure 1**, in which steps are described later and using the specified precursors and solvents.

2.1. Materials

All reactives were analytic degree: natural graphite powder, sulfuric acid 98% (H_2SO_4), hydrochloric acid (HCl), acetone, ethanol 98%, sodium nitrate ($NaNO_3$), and potassium permanganate ($KMnO_4$) from Meyer. Aniline monomer and gold (III) chloride trihydrate ($HAuCl_4{\cdot}H_2O$) and polytetrafluoroethylene (PTFE) were purchased from Sigma Aldrich. The hydrogen peroxide (30% H_2O_2) was purchased from Reasol, and ammonium persulfate (APS) was from Golden Bell.

2.2. Synthesis of graphene oxide sheets

Graphite oxide (GO) was synthesized by a modified Hummer's method [11]. Graphite (10 g), $NaNO_3$ (5 g), and concentrated H_2SO_4 (230 ml) were mixed and stirred at 0°C in a 2000 ml reaction flask, which was immersed in an ice bath. Then, $KMnO_4$ (30 g) was added gradually over the stirring mixture, the temperature was controlled below 35°C, and the whole mixture was stirred for 2 h. After 30-min rest, the temperature of the mixture was raised to 98°C, and 460 ml of de-ionized water was slowly added to the suspension during 40 min.

After 30 min, the mixture was diluted by 1.4 l of de-ionized water and treated with (25 ml) H_2O_2 30% to reduce residual permanganate to soluble manganese ions until the gas evolution ceased. The resulting suspension was washed with HCl 1 M and de-ionized water until the filtrate became neutral and remaining impurities were removed. The product, graphite oxide, was exfoliated in an ultrasonic bath (2 h) to form graphene oxide (GO) sheets.

2.3. Synthesis of polyaniline nanofibers and in situ polymerization GO/PANI

Polyaniline was synthesized by chemical polymerization using ammonium persulfate (APS) as oxidant and HCl as doping agent. The aniline and APS mole ratio employed was 1:1, dissolved

in 100 ml HCl 2 M separately, and put into an ice bath. The two solutions were mixed rapidly at 20°C temperature and put in ultrasonic bath for 3 h. The obtained green mixture was filtered and washed with ethanol and de-ionized water. The final product was put into a vacuum oven at 60°C for 4 h.

The polyaniline/graphene oxide (GO/PANI) composite was prepared by the same polymerization method with the presence of graphene oxide. In this case, the aniline was fixed at 40% wt. with 60% wt. graphene oxide in the acidic solution of HCl 2 M, according to the method reported and mentioned before [11].

2.4. Synthesis of Au nanoparticles (AuNp)

In a flask with 10 ml of 1 mM $HAuCl_4$ brought to boil with vigorous stirring, rapid addition of 1 ml of 38.8 mM sodium citrate to the vortex of the solution was added and resulted in a color change from yellow to burgundy. The heating at the same temperature and stirring was continued for an additional 15 min, and the resulting colloidal particles solution was stored at 4°C.

2.5. Electrodes and electrochemical measurement

To prepare the working electrode samples, GO, PANI or GO/PANI, and PTFE were mixed (90:10, w/w) and dispersed in ethanol. For the system GO/PANI, AuNp, and PTFE, they were mixed (72:20:8%), respectively, and were also dispersed by sonication in ethanol. Carbon cloth, stainless steel, and copper electrode (1 cm^2 area) were coated with the mixture and dried at room temperature for 12 h.

The electrochemical experiments were performed in a three electrode cell arrangement. A graphite rod was used as a counter electrode, and the potentials were measured with respect to a Ag/AgCl standard electrode (saturated with KCl). The electrochemical impedance measurements were carried out by applying an AC voltage of 10 mV amplitude in the 10 kHz–0.01 Hz frequency range. Cyclic voltammetry measurements were carried out in 1 M H_2SO_4 solution at different scan rates of 2–100 mV/s in a voltage range of −0.4 to 1.2 V. Electrochemical Gill AC Instruments analyzer ACM serial 1039 were used throughout the experiments.

3. Characterization of the hybrid materials

To realize the characterization of the synthesized hybrid materials, they were analyzed with the relevant methods and specified instruments.

3.1. Apparatus

Morphological characterization was carried out by using SEM Hitachi S-5500. The X-ray diffraction patterns were obtained from a Bruker D2 Phaser. The FTIR infrared analysis was measured with Platinum-ATR Alpha Bruker, and the ultraviolet visible spectra were obtained from Genesys 105 UV-Vis Thermo Scientific. Scanning electron microscope (SEM) was a LEO

http://dx.doi.org/10.5772/intechopen.77385

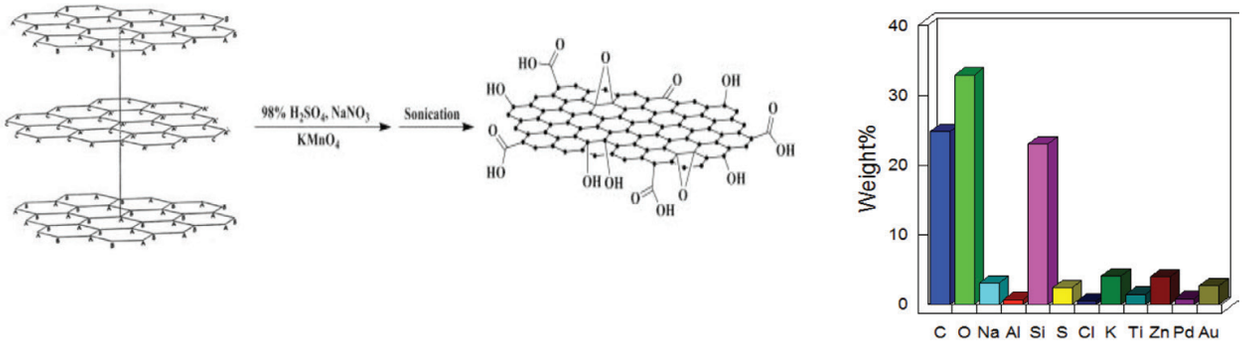

a) b)

Figure 2. (a) GO sheets separation and (b) elemental analysis.

model operating at 15 kV, at 1, 5, 10, and 15 kX magnifications. Raman spectroscopy was a WITec alpha 300 AR, laser source: 532 nm (green), power: 15.6 mW, optical objective: 100×, integration time 5 s, eight accumulations.

3.2. Elemental analysis of the GO

As was mentioned in the methodology description, to obtain GO sheets, graphite was previously oxidized by a modified Hummer's method [11] consisting in the chemical oxidation of the structure through the use of concentrated sulfuric acid, potassium permanganate, and sodium nitrate. After oxidation, this was followed by ultrasonic bath, to break Van der Waals forces to separate the sheets and to obtain GO (**Figure 2a**). The incorporation of oxygen into the graphite crystalline network was corroborated, determining the carbon/oxygen ratio through SEM elemental X-ray analysis (**Figure 2b**).

3.3. FTIR spectroscopy

FTIR spectroscopy was used to elucidate the covalent grafting and to confirm the change in functional groups during each step. **Figure 3** represents the FTIR spectra of GO, PANI, GO/PANI, and GO/PANI/AuNp. The GO shows absorption bands at 3200 and 1734 cm^{-1}, which correspond to O—H, C=O in COOH [12]. It can be also observed that there are bands around 1605 and 1376, which are due to the intercalated water and deformation vibrations of C—O in C—OH and C—O—C functional groups [13].

For pure PANI prominent attributed absorption peaks are seen at 1630 and 1394 cm^{-1}, belonging to C=C stretching deformation of quinoid and C=N stretching of secondary aromatic amine, revealing the presence of emeraldine salt state in PANI [14]. The bands at 1184 and 805 cm^{-1} correspond to —C—N stretching vibration and out of plane bending vibrations of C—H in the benzene ring. Around 3281 cm^{-1}, it was observed an absorption band for N—H stretching of the amine group.

The FTIR spectrum of the GO/PANI composite was identical to that of PANI, which confirmed that the GO surface was wrapped by PANI [14]. There is no peak observed at 3200 and 1734 cm^{-1} (—OH and C=O vibrations, respectively), indicating the reduction of GO took

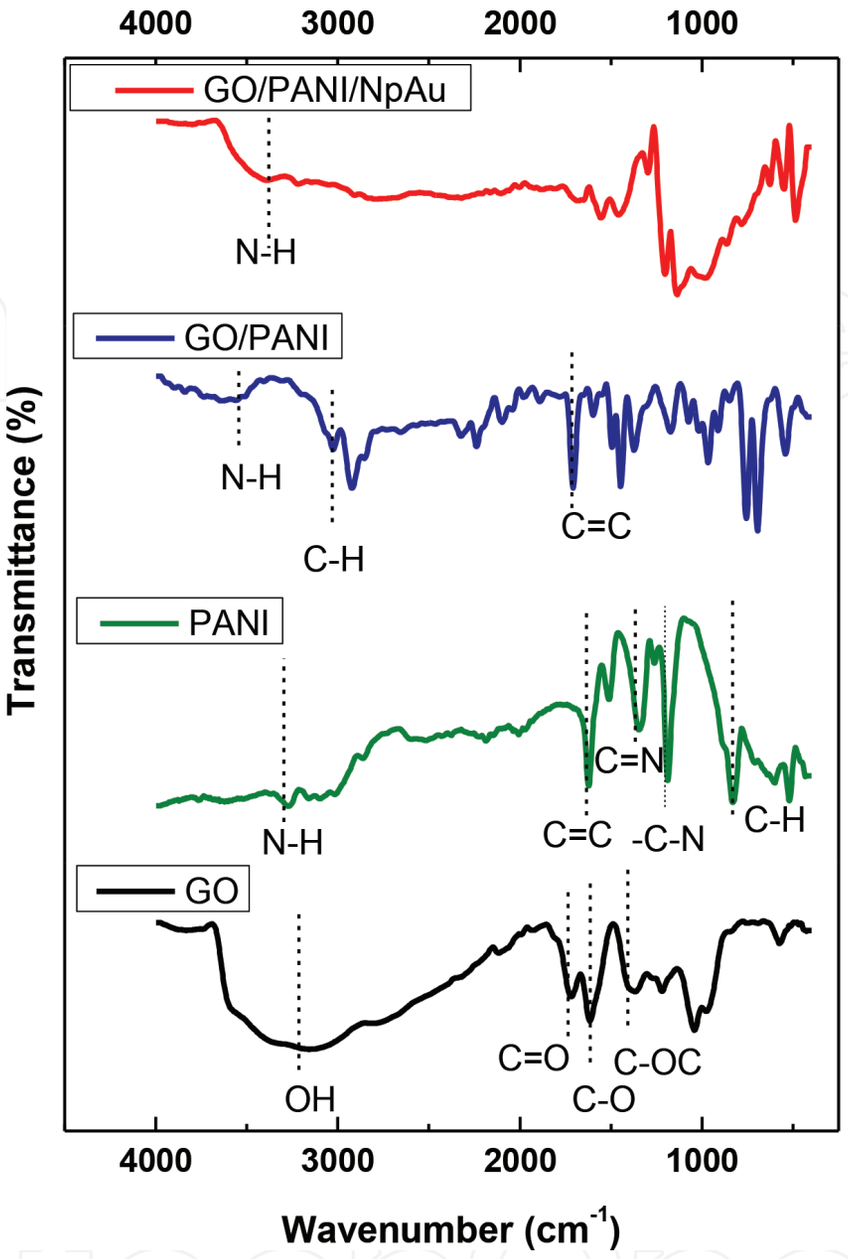

Figure 3. FT-IR spectrum of GO, PANI, and the composites GO/PANI and GO/PANI/AuNp.

place due to the polymerization of aniline, in addition to the confirmation that PANI has been covalently grafted onto the surface of the GO sheets. The FTIR bands were displaced, indicating a covalent bond and displacement due to the molecule arrangement. Functional groups responsible for stabilization of gold nanoparticles appeared in the band at 3300 cm^{-1} corresponding to N—H vibrations [15].

3.4. X-ray diffraction

Understating the morphological as well as structural changes of the products obtained, XRD studies on graphite, GO, PANI, GO/PANI, and GO/PANI/AuNp were analyzed.

http://dx.doi.org/10.5772/intechopen.77385

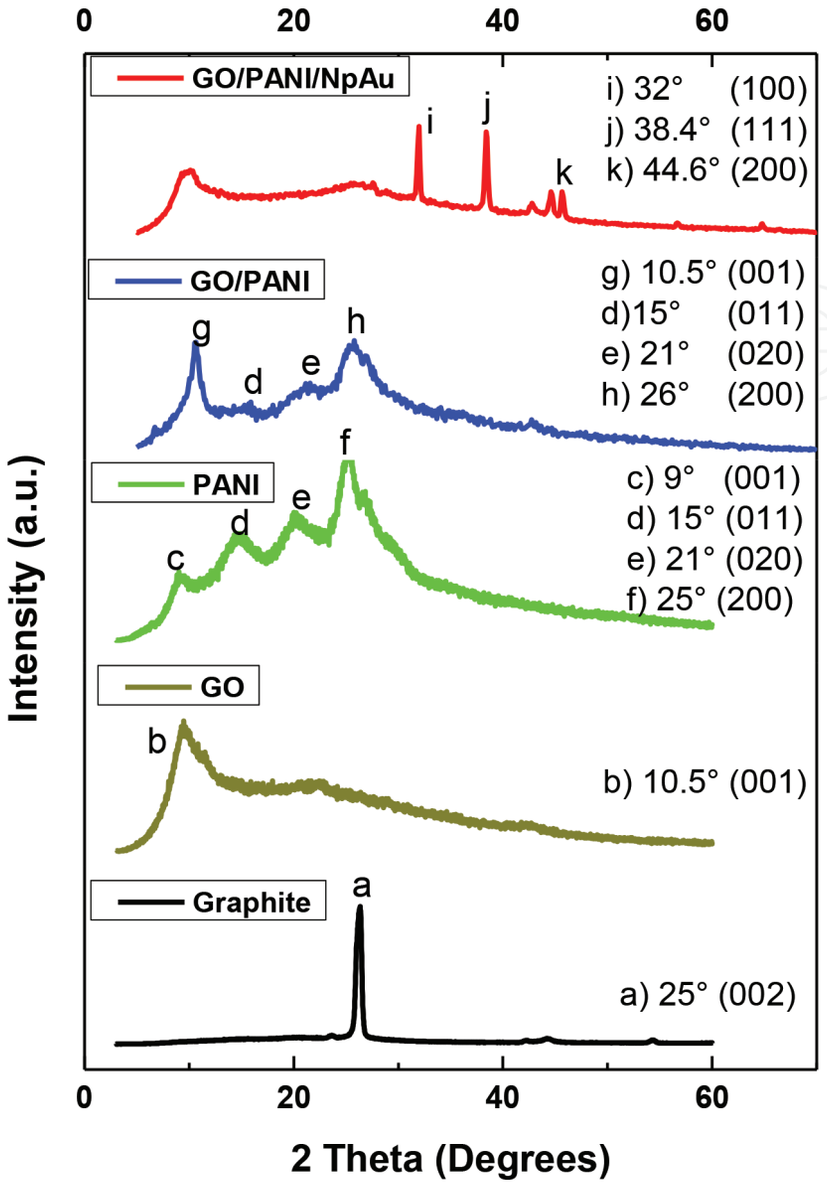

Figure 4. X-ray diffraction (XRD) of graphite, GO, PANI, GO/PANI, and GO/PANI/AuNp.

Figure 4 exhibits the XRD crystallographic pattern of graphite, and the basal reflection (002) peak at 2θ = 25° indicates a d-spacing of 0.35 nm based on Bragg's equation. After chemical oxidation, the peaks shifted to a lower angle reflection plane (001) at 2θ =10.5°, which indicates a d-spacing of 0.84 nm.

This widening of the d-spacing can be attributed to the intercalation of water molecules and generation of oxygenated functional such as epoxy, hydroxyl, and carboxyl groups between the inter-layering of the graphite sheets during severe oxidation [9], the small peak observed at 2θ = 42.5° associated with (100) plane of graphite, and indicates that small amounts of graphite phases are still present [10]. The peaks for emeraldine form PANI were exhibited at 2θ = 25, 21, 15, and 9° corresponding to (200), (020), (011), (001) reflections for PANI, respectively [16].

After the polymerization, it is observed the reduction of graphene oxide by the interaction with PANI demonstrated with the decrease of (001) reflection plane angle (2θ = 10.5°). The XRD pattern of GO/PANI presents crystalline peaks similar to those of PANI. The peak around 2θ = 26° is correlated to the interlayer space between the graphene sheets, which overlap with the diffractions from PANI [16]. The AuNp peaks were observed at 2θ = 32, 38.4, and 44.6°, corresponding to (100), (111), and (200) planes of the face centered cubic crystal, respectively.

3.5. Ultraviolet-vis

The AuNps were synthesized by Turkevich's method (1951) [17] in which reduction results were observed with the color change from pale yellow to burgundy. The color of AuNp is dependent upon the size and shape of the nanoparticles formed, which is correspondingly associated with the surface plasmon resonance due to collective oscillations of six electrons in the conduction band of AuNp, and this is the resonance frequency of the incident electromagnetic radiation [17, 18]. In **Figure 5a**, the burgundy particle dispersion attributed to circular shape particles with less than 40 nm in size can be observed, which agreed with circular shape with diameters 10-40 nm for AuNp, obtained by the citrate method [19].

The maximum absorption was observed at 520 nm (as seen in **Figure 5b**) corresponding to the plasmon collective oscillation of gold [20], indicating that the nanoparticles are evenly dispersed in the aqueous solvent. When the incident light wave frequency resonates with the electron coherent movement from the conduction band, it produces a strong absorption, which is the origin of the observed colloidal color [21]. For small metallic nanoparticles (less than 20 nm in diameter), the absorption spectrum only depends on the dipole oscillation, being the reason for the color change from the Au salt reaction (pale yellow) with the sodium citrate, forming gold nanoparticles (burgundy color), in which the resonant maximum absorption band of plasmon surface (520 nm) observed is AuNp characteristic nuclei response.

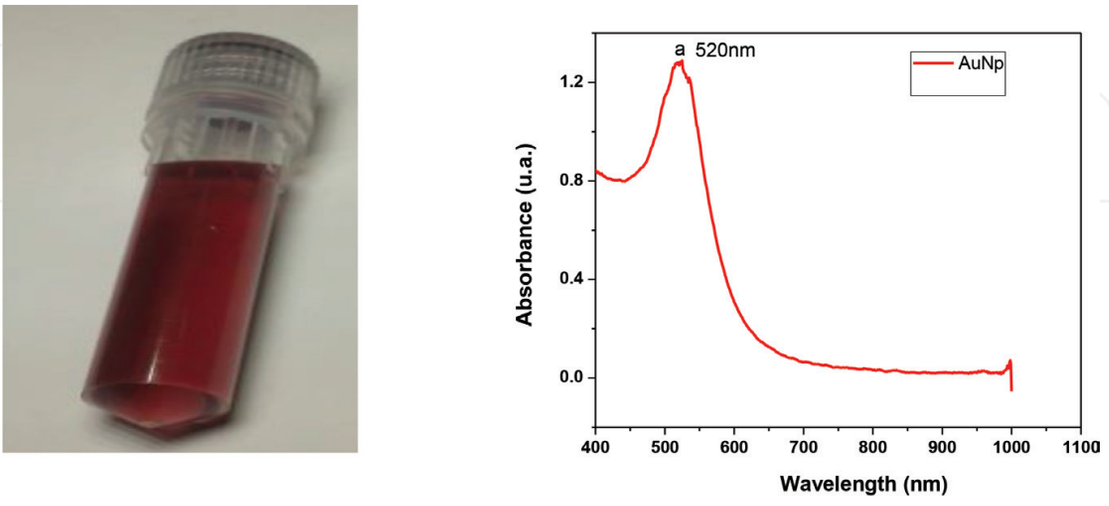

a) b)

Figure 5. UV-Vis of gold nanoparticles (a) nanoparticles dispersion and (b) the maximum absorption observed at 520 nm.

http://dx.doi.org/10.5772/intechopen.77385

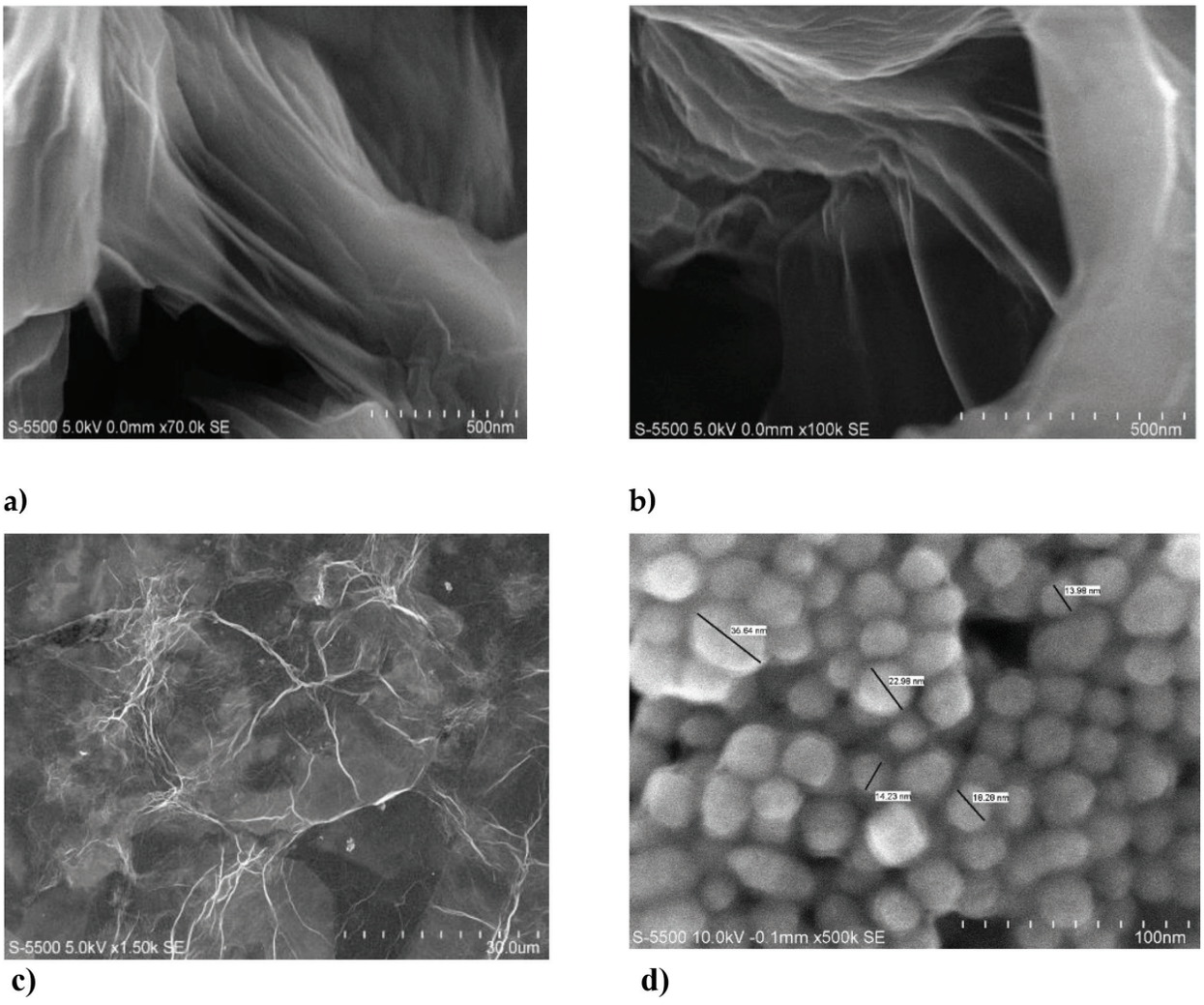

Figure 6. HRSEM micrographs of (a–c) graphene oxide and (d) gold nanoparticles.

3.6. High-resolution scanning electron microscopy

High-resolution scanning electron microscopy (HRSEM) images were used to study size, shape, and dispersion about the synthesized nanomaterials. **Figure 6(a–c)** presents SEM micrographs at different magnifications showing views of the GO obtained by Hummer's modified method, graphene oxide sheets morphology are clearly seen, showing wrinkled and folded regions and the transparent property associated with them. Surface properties are associated with the shape and size of AuNp (**Figure 6d**) presenting sphere particles with an average size of 10–40 nm in diameter.

3.7. Raman spectroscopy

Raman spectroscopy is one of the most important techniques to detect and distinguish the graphene properties. This technique provides valuable information regarding the number of sheet layers, edges, and defects. This evaluation is very important because structural defects transform the graphene in such a way that intrinsic defects in the band structure modify its electric and magnetic properties.

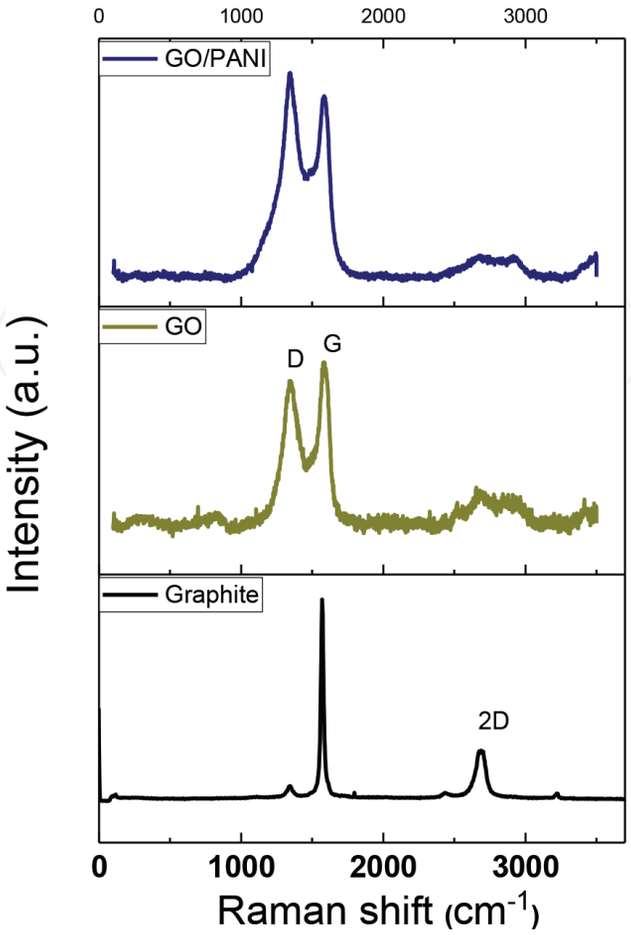

Figure 7. Raman spectra of graphite, GO, and GO/PANI composite.

Figure 7 shows the Raman spectra of graphite, GO, and GO/PANI composite. Graphite exhibits two peaks: a *D* band at 1363 cm^{-1} corresponding to defects or edge areas and a *G* band at 1577 cm^{-1} related to the vibration of sp^2-hybrided carbon. When GO is intercalated and oxidized, the band shifts to a higher wavenumber (1589 cm^{-1}) and widens as a result of a loss of interaction between the adjacent layers. The band of GO/PANI at 1358 cm^{-1} is more intense than that of GO due to the intercalation of oxygen-containing functional groups with covalent bonding in the GO layer [13, 14].

4. Electrochemical properties of the hybrid materials

4.1. Electrochemical capacitors

Electrochemical impedance spectroscopy (EIS) analysis was then carried out to investigate the electrochemical behavior of the materials synthesized. Hybrid coatings were tested first in carbon cloth acting as a substrate (blank). A typical Nyquist plot consisted of a semicircle in the high-frequency region and a linear part in the low-frequency area is formed [22]. Alternatively, the Bode plot presents the total impedance and phase angle as a function of frequency.

The diameter of the semicircle correlates with the interfacial charge-transfer resistance, usually representing the electrochemical reaction on the electrode (Faradaic resistance) [23]. All

http://dx.doi.org/10.5772/intechopen.77385

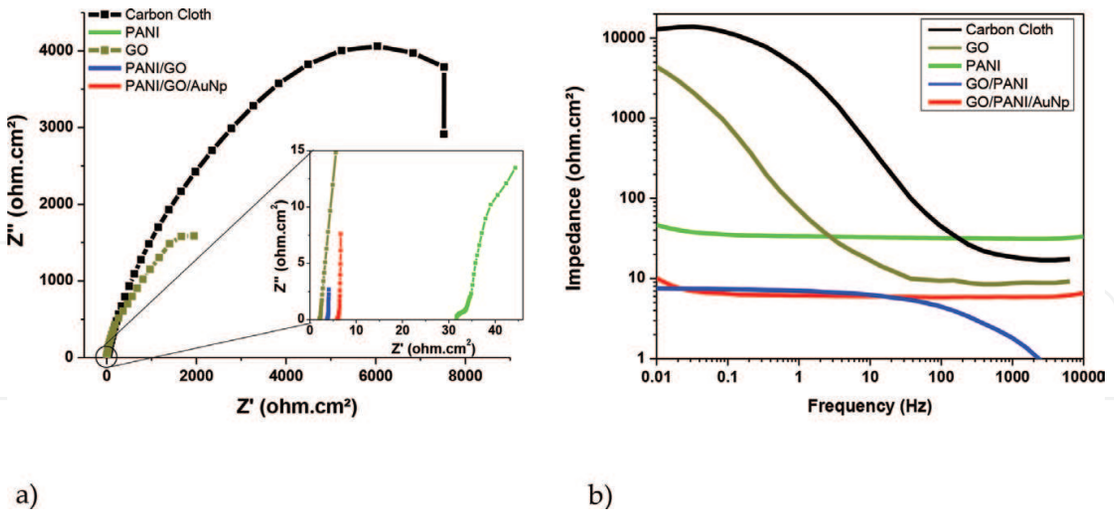

Figure 8. Impedance plots (a) Nyquist and (b) Bode for carbon cloth material support, and each synthesized material; GO, PANI, GO/PANI, GO/PANI/NpAu.

hybrid materials show very small diameter semicircle demonstrating the good electrical conductivity of the three-element composite, with a semi-straight line at mid to low frequencies, associated to capacitive behavior (mass transfer control) and lower charge-transfer resistance.

The Nyquist and Bode plots obtained are presented in **Figure 8a** and **b**, respectively, and for comparison purposes, the carbon cloth presents the highest overall or total impedance value above 1 kohm·cm^2 at the low frequency limit (0.01 Hz). The GO system shows a lower impedance value around 4500 kohms·cm^2, both showing an inverse frequency behavior at intermediate frequencies corresponding to double layer capacitance. For the PANI system, the impedance values diminished in all the frequency bandwidth considered around 45 ohms·cm^2, reflecting the conductive properties of the polymer material.

The GO/PANI/AuNp hybrid exhibits the semicircle smaller than GO/PANI and PANI, suggesting better conductivity and lower charge transfer resistance. A straight sloping line in the lower frequency represents the diffusion resistance (Warburg impedance, W), which reflects the diffusion or mass transfer of redox species in the electrolyte, and a steeper line usually indicates faster ion diffusion.

Based on these electrochemical analyses, the enhanced capacitive behavior was due to the synergistic effect between graphene oxide and PANI, besides the high conductivity of the AuNp. In addition, the small nanometer size can exhibit enhanced electrode/electrolyte interface areas, providing high electro-active regions and short diffusion lengths. This is also true for the GO/PANI and GO/PANI/AuNp hybrid materials showing a further decrease of around 10 ohms·cm^2, presenting low impedance behavior all around [22].

Bode impedance diagrams (**Figure 8**) demonstrate that the synthesized materials PANI, GO/PANI, and GO/PANI/AuNp present good conductivity properties with low impedance values. Also, the capacitive behavior was observed with the carbon cloth (blank) and the GO material. This analysis reveals that the good electrical conductivity and ion diffusion behavior resulted in the electrochemical performance of GO/PANI/AuNp of the three element hybrid material [23].

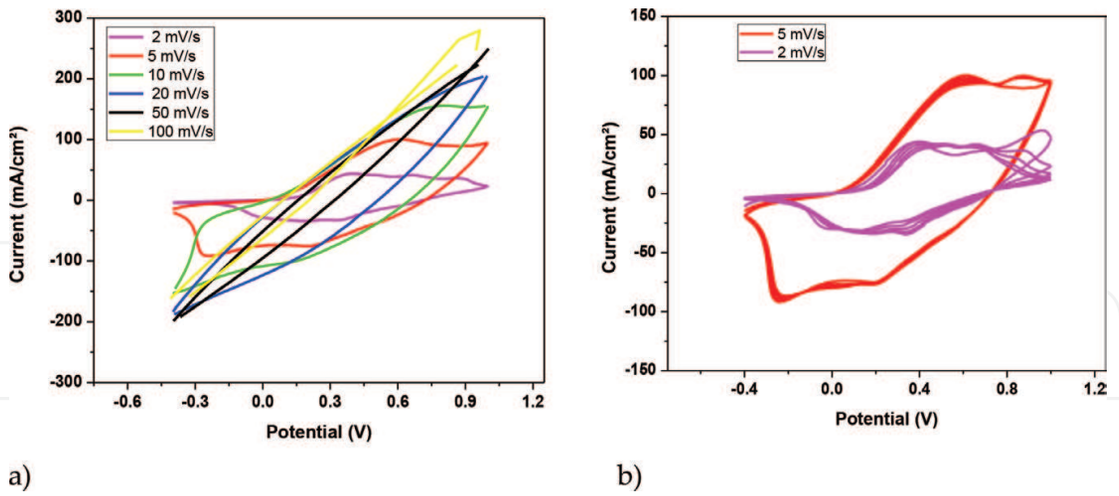

Figure 9. Cyclic voltammetry results of (a) carbon cloth different rates and (b) carbon cloth at 2 and 5 mV/s showing a trapezoidal form.

Another phenomenon that reinforces the theoretical explanation [24] is the reduction of the total impedance about two to three orders of magnitude with respect to the carbon cloth (blank) as can be seen in the Bode impedance diagram (**Figure 8b**), indicating the greatly increased ionic conductivity (high frequency) of the system.

Cyclic voltammetry is a tool used to evaluate the faradaic and nonfaradaic processes as well as the capacitive properties and mechanisms of reaction at the electrode interface (**Figure 9**). The electrochemical response of the carbon cloth, of current as a function of potential for different sweep rates, is shown (**Figure 9a**), obtaining the best rate at 5 mV/s, where a more trapezoidal shape was obtained (**Figure 9b**).

Figure 10a presents the cyclic voltammetry of carbon cloth coated with polyaniline (PANI) showing oxidation peaks for PANI around 0.5 and 0.96 V, while reduction peaks are observed at −0.2 and 0.2 V. The separation between peaks is more than 0.2 V; therefore, the reaction is quasi-reversible and attributed to transition of PANI, from emeraldine to the pernigraniline form [25]. The incorporation of PANI as a cover demonstrates the increased capacitance from the shape obtained.

In **Figure 10b**, the cyclic voltammogram for the different components applied to the carbon cloth supporting material (blank) in a (H_2SO_4) 1 M solution is presented. The graphs show when incorporating the PANI to the GO matrix the current increases about 63 mA/cm^2 as the maximum peak in the anodic current (ia), while an increase in 100 mA/cm^2 is observed as the maximum peak, for the whole hybrid system GO/PANI/AuNp. The subsequent incorporation of the different components to the hybrid system increases the total area of the trapezoid shape.

This involves two types of capacitive behavior contribution: from the electrochemical double layer capacitance (EDL) produced by GO and pseudo capacitive behavior from the incorporation of PANI. This suggestion is obtained from the two peaks observed in the voltammogram that indicated the existence of faradaic processes. This suggests a good synergism from the components of the matrix as well as good conductive properties [26].

http://dx.doi.org/10.5772/intechopen.77385

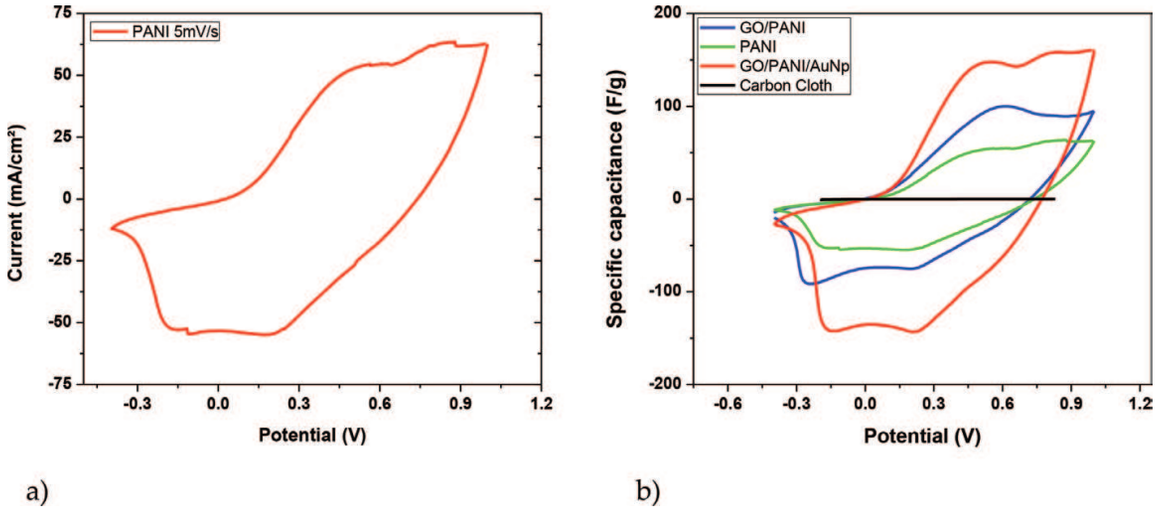

Figure 10. Cyclic voltammetry results of (a) PANI showing redox peaks to transition of PANI, from leucoemeraldine/emeraldine and emeraldine/pernigraniline form and (b) carbon cloth, PANI, GO/PANI, and GO/PANI/AuNp.

The specific capacitance of the electrodes can be calculated according to the following equation (1) from CV curves:

$$C = \frac{I}{mV} \tag{1}$$

where I is the current, m is the mass of reactive material, and V is the potential scan rate.

The system presents potential to be used as capacitors with obtained values around 100–160 F/g. Au nanoparticles improve the capacitance behavior in GO/PANI/AuNp hybrid material for energy application.

4.2. Fuel cell electrodes

Another interesting possibility for the hybrid material synthesized may have promising applications as conductive material such as electrodes for fuel cells, in combination with metallic substrates. In the following examples, metal substrate includes copper and stainless steel [27].

For stainless steel substrate with the four synthesized hybrid component as coatings, immersed in the H_2SO_4 solution, the Nyquist and Bode impedance plots are presented in **Figure 11**. The two time constant behavior can be seen. The coatings response and dielectric properties are ascribed to higher frequencies (kHz), whereas at mid to lower frequencies (Hz–mHz), the response is associated with the oxide layer or bare metal substrate coating interface [28]. For the system tested, Nyquist plots present small diameter semicircle followed by a straight line with different slopes, corresponding to mass transfer diffusion process (**Figure 11a**). Bode plots (**Figure 11b**) present at the highest frequency: in the PANI coated stainless steel the highest impedance (70 ohms·cm2), followed by GO, GO/PANI, PANI and the lowest for GO/PANI/AuNp (10 ohms·cm^2).

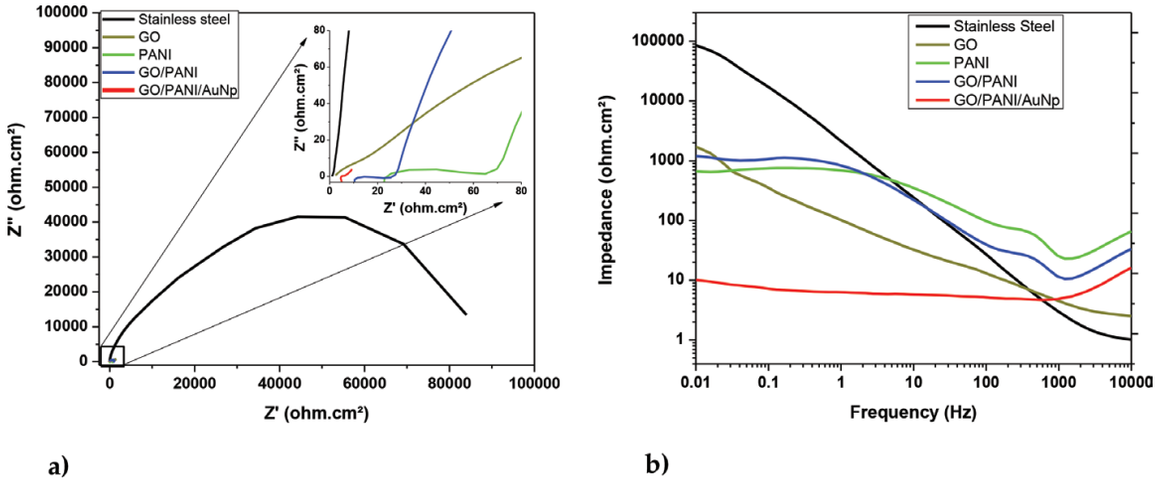

Figure 11. Impedance for stainless steel and different coating components immersed in H_2SO_4 1 M solution (a) Nyquist and (b) Bode plots.

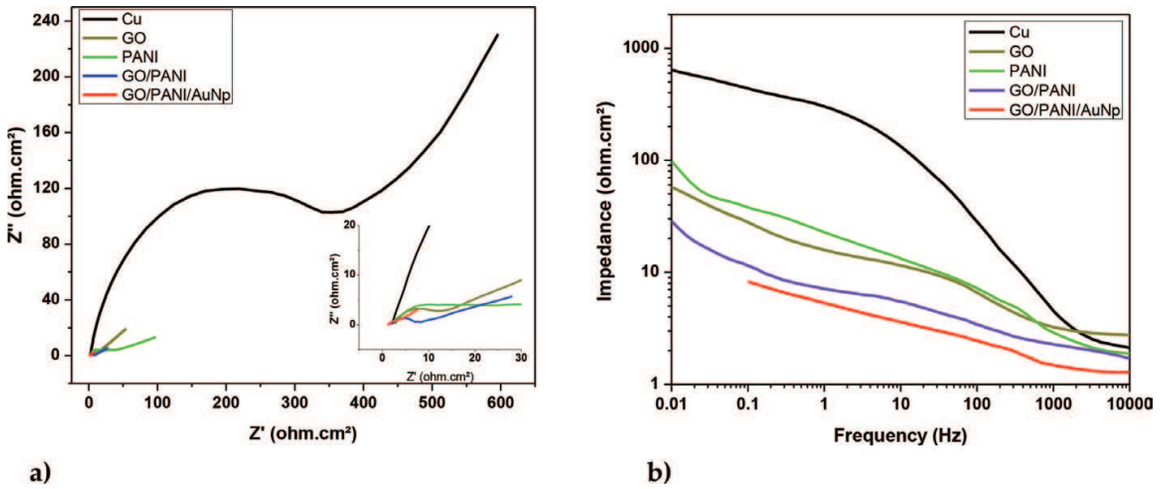

Figure 12. Impedance for copper and different coating components immersed in H_2SO_4 1 M solution (a) Nyquist and (b) Bode plots.

In a similar way as before, the coating systems were applied, but this time in a copper metal substrate. A similar response was obtained (**Figure 12**), where the Nyquist plots show a semicircle with lower impedance resistance values as compared with stainless steel samples; followed by a straight line with different slopes associated to the coating protection and mass transport (**Figure 12a**) [29].

The high frequency impedance obtained was for the GO, followed by Cu, PANI, GO/PANI, and the lowest impedance value (15 ohms·cm^2) for the GO/PANI/AuNp coating sample. The highest impedance modulus (low frequency) seen is for the bare copper sample (650 ohms·cm^2) lowering its values for PANI, GO, and GO/PANI, and the smallest value registered is for the coating GO/PANI/AuNp system (**Figure 12b**). The mass transfer is reflected in the impedance modules obtained [30].

http://dx.doi.org/10.5772/intechopen.77385

Both metal coating systems present good conductive properties for the hybrid synthesized coating system. Lower resistance, good ionic conductivity, and capacitive properties, which present GO/PANI/AuNp compound, make it attractive for different technological developments and applications in the energy sector.

5. Summary

It was possible to synthesize the hybrid material as evidenced by the characterization techniques. Electrochemical analysis demonstrates the capacitive redox behavior of PANI, but graphene, which is a material with large surface area (the property that increases the capacitance) when combined with the polyaniline conducting polymer, acts as a good material for electrical conduction rather than good capacitive behavior. The introduction of the AuNp in the network further increases the electric conduction. The trapezoidal shape of the voltammetric curves indicates maximum peaks with a capacitance of 160 F/g. This quantity indicates that the current is delivered very fast, which is not convenient for a capacitor. These results conclude that it is not a very good material for energy storage; however, it has promising applications as conductive material such as electrodes for fuel cells. Good electrochemical properties were obtained for metal electrodes coated with the hybrid systems, suggesting good energy electrode applications.

Acknowledgements

The authors wish to thank SEP-PROMEP for the support provided to both the Academic Body "Desarrollo y Análisis de Materiales Avanzados" (UAEMOR-CA-43) and the Academic Network "Diseño Nanoscópico y Textural de Materiales Avanzados." Finally, the authors thank CONACyT for the student grants received during this work.

Conflict of interest

The authors confirm that this content has no conflict of interest.

Author details

Carmina Menchaca-Campos[1], Elsa Pereyra-Laguna[1], César García-Pérez[1], Miriam Flores-Domínguez[1], Miguel A. García-Sánchez[2] and Jorge Uruchurtu-Chavarín[1]*

*Address all correspondence to: juch25@uaem.mx

1 Centro de Investigación en Ingeniería y Cciencias Aplicadas-(IICBA), Universidad Autónoma del Estado de Morelos, Cuernavaca, Morelos, Mexico

2 Departamento de Química, UAM-Iztapalapa, Mexico, DF, Mexico

References

[1] Fan W, Zhang C, Tjiu WW, Pramoda KP, He C, Liu T. Graphene-wrapped polyaniline hollow spheres as novel hybrid electrode materials for supercapacitor applications. ACS Applied Materials and Interfaces. 2013;**5**:3382-3391. DOI: 10.1021/am4003827

[2] Wu H, Zhang Y, Cheng L, Zheng L, Li YQ, Yuan W, Yuan X. Graphene based architectures for electrochemical capacitor. Energy Storage Materials. 2016;**5**:8-32. DOI: 10.1016/j.ensm 2016.05.003

[3] Sun H, She P. Xu K, Shang Y, Yin S, Liu Z. A self-standing nanocomposite foam of polyaniline reduced graphene oxide for flexible super-capacitor. Synthetic Metals. 2015;**209**:68-73. DOI: 10.1016/j.synthmet.2015.07.001

[4] Chen N, Ren Y, Kong P, Tan L, Feng H, Luo Y. In situ one-pot preparation of reduced graphene oxide/polyaniline composite for high performance electrochemical capacitor. Applied Surface Science. 2017;**392**:71-79. DOI: 10.1016/j.apsusc.2016.07.168

[5] Gupta S, SG P. Investigating graphene/conducting polymer hybrid layered composites as pseudocapacitors: Interplay of heterogeneous electron transfer, electric double layer and mechanical stability. Composites Part B Engineering. 2016;**105**:46-59. DOI: 10.1016/j.compositesb.2016.08.035

[6] Thirumal V, Pandurangan A, Jayavel R, Ilangovan R. Synthesis and characterization of boron doped graphene nanocheets for supercapacitor applications. Synthetic Metals. 2016;**220**:524-532. DOI: 10.1016/j.synthmet.2016.07.011Get

[7] West RM, Semancik S. Interpenetrating polyaniline-gold electrodes for SERS and electrochemical measurements. Applied Surface Science. 2016;**387**:260-267. DOI: 10.1016/j.apsusc.2016.06.073

[8] Liu Q, Nayfeh O, Nayfeh MH, Yao ST. Flexible supercapacitor sheets based on hybrid nanocomposite materials. Nano Energy. 2013;**2**:133-137. DOI: 10.1016/j.nanoen.2012.08.007

[9] Xiong P, Zhu J, Wang X. Recent advances on multi-component hybrid nanostructures for electrochemical capacitors. Journal of Power Sources. 2015;**294**:31-50. DOI: 10.1016/j.jpowsour.2015.06.062

[10] Shayeh JS, Ehsani A, Ganjali MR, Norouzi P, Jaleh JB. Conductive polymer/reduced graphene oxide/Au nano particles as efficient composite materials in electrochemical supercapacitor. Applied Surface Science. 2015;**353**:594-599. DOI: 10.1016/j.apsusc.2015.06.066

[11] Fernández PS. Modificación superficial de materiales de carbono: grafito y grafeno. Universidad de Oviedo; 2011. http://hdl.handle.net/10651/12792

[12] Xu Y, Liu Z, Zhang X, Wang Y, Tian J, Huang Y, Ma YY, Zhang X, Chen Y. A graphene hybrid material covalently functionalized with porphyrin: Synthesis and optical limiting property. Advanced Materials. 2009;**21**:1275-1279. DOI: 10.1002/adma.200801617

[13] Hu F, Li W, Zhang J, Meng W. Effect of gaphene oxide as a dopant on the electrochemical performance of graphene oxide/polyaniline composite. Journal of Materials Science and Technology. 2014;**30**:321-327. DOI: 10.1016/j.jmst.2013.10.009

[14] Kumar M, Singh K, Dhawan SK, Tharanikkarasu K, Chung JS, Kong BS, Kim EJ, Seung JK, Hur H. Synthesis and characterization of covalently-grafted graphene-polyaniline nanocomposites and its use in a supercapacitor. Chemical Engineering Journal. 2013;**231**:397-405. DOI: 10.1016/j.cej.2013.07.043

[15] Eisa WH, Zayed MF, Abdel-Moneam YK, Zeid AMA. Water-soluble gold/polyaniline core/shell nanocomposite: Synthesis and characterization. Synthetic Metals. 2014;**195**:23-28. DOI: 10.1016/j.synthmet.2014.05.012

[16] Zhao M, Wu X, Cai C. Polyaniline nanofibers: Synthesis, characterization and applications to direct electron transfer of glucose oxidase. Journal of Physical Chemistry. 2009;**113**:4987-4996. DOI: 10.1021/jp807621y

[17] Chen M, He Y, Liu X, Zhu J. Synthesis and optical properties of size-controlled gold nanoparticles. Powder Technology. 2017;**311**:25-33. DOI: 10.1016/j.powtec.2017.01.087

[18] Gharatape A, Salehi R. Recent progress in theranostic applications of hybrid gold nanoparticles. European Journal of Medicinal Chemistry. 2017;**138**:221-233. DOI: https://doi.org/10.1016/j.ejmech.2017.06.034"\t"_blank"\o "Persistent link using digital object identifier" 10.1016/j.ejmech.2017.06.034

[19] Grabar KC, Freeman RGW, Natan MJ, Khatherine C. Preparation and characterization of Au colloid monolayers. Analytical Chemistry. 1995;**67**:735-743. DOI: 0003-2700/95/0367-0735$9

[20] Hyperlink"https://www.sciencedirect.com/science/article/pii/S2405580817301103"\l "%21" Santhoshkumar Hyperlink "https://www.sciencedirect.com/science/article/pii/S2405580817301103"\l"%21"S.RajeshkumarHyperlink"https://www.sciencedirect.com/science/article/pii/S2405580817301103" \l "%21" Santhoshkumar J, Rajeshkumar S, Kumar SV. Phyto-assisted synthesis, characterization and applications of AuNPs–A review. Biochemistry and Biophysics Reports. 2017;**11**:46-57. DOI.org/10.1016/j.bbrep.2017.06.004 DOI: "https://doi.org/10.1016/j.bbrep.2017.06.004" \t "_blank" \o "Persistent link using digital object identifier" 10.1016/j.bbrep.2017.06.004

[21] Hyperlink"https://www.sciencedirect.com/science/article/pii/S0022231315004834" \l"%21"DasR,Hyperlink"https://www.sciencedirect.com/science/article/pii/S0022231315004834" \l "%21" Sarkar S, Hyperlink "https://www.sciencedirect.com/science/article/pii/S0022231315004834" \l "%21" Saha M, Hyperlink "https://www.sciencedirect.com/science/article/pii/S0022231315004834" \l "%21". Dey PC, Nath SS. Hyperlink "javascript:void(0)" Two peak luminescence from linoleic acid protected gold nanoparticles. Journal of Luminescence. 2015;**168**:325-329. DOI: Hyperlink "https://doi.org/10.1016/j.jlumin.2015.08.047" \t "_blank" \o "Persistent link using digital object identifier" 10.1016/j.jlumin.2015.08.047

[22] Hyperlink"https://www.sciencedirect.com/science/article/pii/S245191031630031X" \l "%21" Pajkossy T, Hyperlink"https://www.sciencedirect.com/science/article/pii/S245191031630031X" \l "%21" Jurczakowski R. Electrochemical impedance spectroscopy in interfacil studies. Current Opinion in Electrochemistry. 2017;**1**:53-58. DOI: Hyperlink "https://doi.org/10.1016/j.coelec.2017.01.006" \t "_blank" \o "Persistent link using digital object identifier" 10.1016/j.coelec.2017.01.006

[23] Hyperlink "https://www.sciencedirect.com/science/article/pii/S0379677915300096" \l "%21" Sun H, Hyperlink "https://www.sciencedirect.com/science/article/pii/S0379677915300096" \l "%21" She P, Hyperlink "https://www.sciencedirect.com/science/article/pii/S0379677915300096" \l "%21" Xu K, Hyperlink "https://www.sciencedirect.com/science/article/pii/S0379677915300096" \l "%21" Shang Y, Hyperlink "https://www.sciencedirect.com/science/article/pii/S0379677915300096" \l "%21" Yin S, Liu Z. A self-standing nanocomposite foam of polyaniline@reduced graphene oxide for flexible super-capacitor. Synthetic Metals. 2015;**209**:68-73. DOI: Hyperlink "https://doi.org/10.1016/j.synthmet.2015.07.001" \t "_blank" \o "Persistent link using digital object identifier" 10.1016/j.synthmet.2015.07.001

[24] Du W, Wang Z, Zhu Z, Hu S, Zhu X, Shi Y, Pang H, Qian X. Facile synthesis and superior electrochemical performances of CoNi/graphene nanocomposite suitable for supercapacitor electrodes. Hyperlink "https://doi.org/10.1039/2050-7496/2013" \o "Link to journal home page" Journal of materials chemistry A. 2014;**2**:9613-9619. DOI: "https://doi.org/10.1039/C4TA00414K" \t "_blank" \o "Link to landing page via DOI" 10.1039/C4TA00414K

[25] Bustos-Terrones V, Serratos-Álvarez IN, Córdoba-Herrera G, Escobar V, Osiris J, Uruchurtu-Chavarín J, Menchaca-Campos C, Preparación y caracterización del complejo polianilina-fluconazol, como pigmento en un recubrimiento anticorrosivo. Revista Tendencias en Docencia e Investigación en Química. 2016;**2**:QM111

[26] Philip D. Honey mediated green synthesis of gold nanoparticles. Spectrochimica Acta Part A. 2009;**73**:650-653. DOI: Hyperlink "https://doi.org/10.1016/j.saa.2009.03.007" \t "_blank" \o "Persistent link using digital object identifier" 10.1016/j.saa.2009.03.007

[27] García-Pérez C, Menchaca-Campos C, Garcia-Sanchez MA, Pereyra E, Rodriguez O, Uruchurtu J. Nylon/porphyrin/graphene oxide fiber ternary composite, synthesis and characterization. Open Journal of Composite Materials. 2017;**7**:146-165. DOI: 10.4236/ojcm.2017.73009

[28] Hernandez M. Hyperlink "https://www.scientific.net/author/Juan_Genesca_1" Genesca J, Hyperlink "https://www.scientific.net/author/Claudia_Ramos" Ramos C, Hyperlink "https://www.scientific.net/author/Emilio_Bucio" Bucio E, Hyperlink "https://www.scientific.net/author/Jos%C3%A9_Guadalupe_Ba%C3%B1uelos" Bañuelos JG, Hyperlink "https://www.scientific.net/author/Alba_Covelo" Covelo A. Corrosion resistance of AA2024-T3 coated with graphene/sol-gel films. Solid State Phenomena. 2015;**227**:115-118. DOI: "https://doi.org/10.4028/www.scientific.net/SSP.227.115" 10.4028/www.scientific.net/SSP.227.115

[29] Menchaca C, Castañeda I, Soto-Quintero A, Guardián R, Cruz R. García-Sánchez MA, Uruchurtu J. Characterization of a "smart" hybrid varnish electrospun nylon benzotriazole copper corrosion protection coating. International Journal of Corrosion. 2012;**2012**:925958-925967. DOI: 10.1155/2012/925958

[30] Menchaca-Campos C, García-Pérez C, Castañeda I, García-Sánchez MA, Guardián R, Jorge Uruchurtu J. Nylon/graphene oxide electrospun composite coating. International Journal of Polymer Science. 2013;**2013**:621627. DOI: 10.1155/2013/621618